JOURNAL OF PROPULSION AND POWER
Vol. 13, No. 4, July–August 1997

Mach 6 Testing of a Scramjet Engine Model

Takeshi Kanda,* Tetsuo Hiraiwa,† Tohru Mitani,‡ Sadatake Tomioka,† and Nobuo Chinzei§
National Aerospace Laboratory, Kakuda, Miyagi 981-15, Japan

Testing of a subscale scramjet research engine model was carried out in the Mach 6 Ramjet Engine Test Facility of the National Aerospace Laboratory, Kakuda Research Center. The engine had a sidewall compression-type inlet. The fuel was hydrogen. With the attachment of a short strut on the top wall, intensive combustion with high-combustion efficiency was attained, and the engine-produced thrust canceled the drag. The flame was held in the low-velocity region around the step, even after the ignitors had been turned off. When the fuel flow rate was small, there was a different combustion mode with weak combustion and little thrust. The unstart condition seemed to begin around the cowl. Tangential injection of fuel inhibited intensive combustion.

Introduction

STUDY of an aerospace plane is being carried out to create a new transportation system to low Earth orbit. One of the engines that will be used in the aerospace plane, the scramjet, is being studied at the National Aerospace Laboratory, Kakuda Research Center (NAL, KRC), and a subscale scramjet research engine model has been tested under Mach 4 and Mach 6 flight conditions in the Ramjet Engine Test Facility (RJTF) at the center.[1,2]

In a previous test under Mach 6 flight conditions, the engine did not produce thrust. To enhance combustion a short strut was attached to the top wall of the engine. This modification was expected to increase the pressure, decelerate the air, enhance the mixing, and create a recirculation region near the ignitors and the backward-facing step for flame holding. The results of the testing with the short strut are herein presented.

Experimental Apparatus and Methods

Test Facility

The test conditions in the RJTF are shown as follows: Mach number, 5.30; total temperature, 1550 K; total pressure, 4780 kPa; and test duration, 60 s. They correspond to the flight conditions of Mach 6 with a flight dynamic pressure of 64 kPa. Compressed air was heated by a ceramic storage heater. The supersonic nozzle had exit dimensions of 51 by 51 cm. The boundary-layer thickness was 58 mm and the displacement thickness was 20 mm at the engine entrance according to pitot pressure measurement.[3]

Engine Model

Figure 1 shows a schematic diagram of the engine model. In the present testing the engine had a short strut on the top wall. Its height was 50 mm, one-fifth that of the engine model. It had a sidewall compression-type inlet, and the contraction ratio was 3. There was a duct with a constant cross section area between the inlet and the combustor that acted as an isolator. The model had two plasma ignitors,[4] each with 2.5-kW power. It employed oxygen as its working gas. There was no fuel injection from the strut. There was a backward-facing step between the isolator and the combustor for both flame holding and isolation of pressure increase in the combustor. Its height h was 4 mm on the sidewalls, and 2 mm on the top wall.

The fuel, hydrogen, was injected normal to the sidewalls through 24 holes, or tangentially to the sidewalls through 24 holes on the steps; their throat diameter was 1.5 mm. The total temperature of the fuel was approximately 280 K and the total pressure of the fuel varied from 3.6 to 6.3 MPa, according to the fuel flow rate. The pilot fuel was supplied through six holes on the top wall and 94 holes on the sidewalls, the diameter of each being 0.5 mm. Fuel flow rates were measured by metering orifices.

The engine was not cooled. Its walls consisted of tough pitch copper, and the leading edges of the sidewall, the top wall, and the cowl were made of nickel. The inner surface of the top wall of the model coincided with that of the Mach 5.3 nozzle to ingest the boundary layer. The boundary layer occupied one-fifth of the engine height at the entrance of the engine. It simulated the entrance conditions of the engine of the aerospace plane.

Measurements

Wall pressure and temperature at 1 mm from the inner surface of the model were measured. In the present paper the wall pressure P_w is nondimensionalized with the total pressure PO in the reservoir of the wind tunnel of the RJTF. In the following figures the pressure of the top wall was measured along the centerline of the channel. The measurement error of nondimensionalized wall pressure was ± 0.0001 in the inlet, in the divergent part of the combustor (D.C.), and in the nozzle; whereas it was ± 0.0005 in the isolator (Is.) and in the constant duct part of the combustor (C.C.).

Heat flux q was estimated from the rate of wall temperature change measured by thermocouples. The Fourier number was about 0.5 in the present testing, and so the heat flux was expressed as follows[5]:

$$q = \rho c l \left(\frac{\mathrm{d}T}{\mathrm{d}t}\right) \tag{1}$$

Here, ρ, c, l, T, and t denote density, specific heat, thickness of the wall, temperature, and time, respectively. The error of heat flux was $\pm 2.5\%$ in the present testing.

Thrust, lift, and pitching moment were measured by a floating frame force measurement system (FMS). The error of

Presented as Paper 96-0380 at the AIAA 34th Aerospace Sciences Meeting, Reno, NV, Jan. 15–19, 1996; received Aug. 16, 1996; revision received Feb. 1, 1997; accepted for publication Feb. 17, 1997.

*Senior Researcher, Kakuda Research Center, Ramjet Propulsion Research Division. Member AIAA.

†Researcher, Kakuda Research Center, Ramjet Combustion Section, Ramjet Propulsion Research Division. Member AIAA.

‡Head, Kakuda Research Center, Ramjet Combustion Section, Ramjet Propulsion Research Division. Member AIAA.

§Head, Kakuda Research Center, Ramjet Performance Section, Ramjet Propulsion Research Division. Member AIAA.

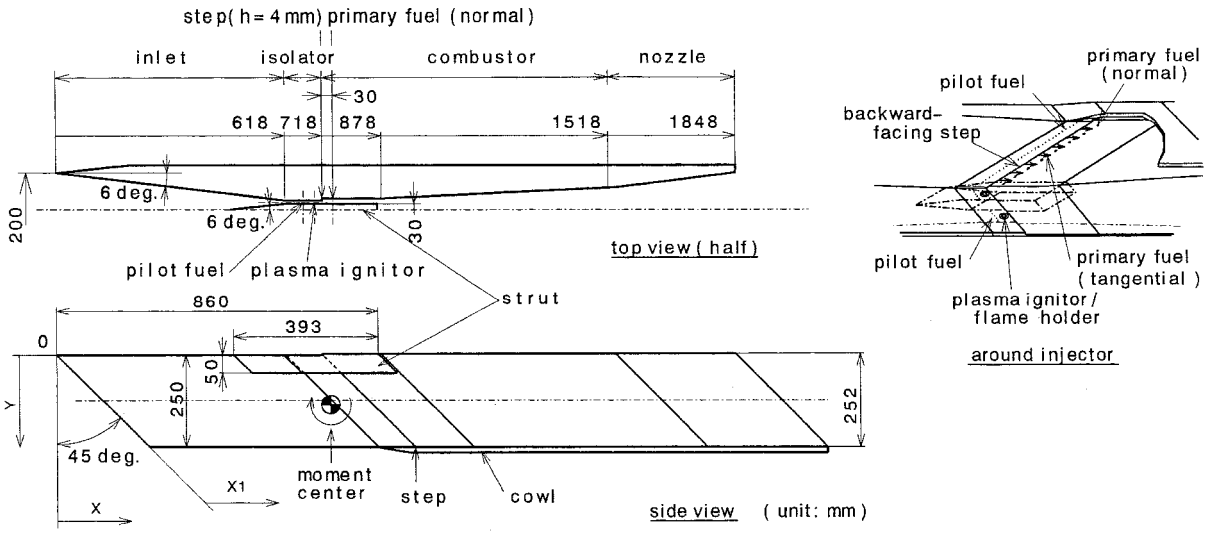

Fig. 1 Engine model.

forces was ±50 N. The center of pitching moment was set at x = 741.43 mm and y = 135.8 mm as shown in Fig. 1. Here, the x coordinate is the distance from the origin as shown in Fig. 1, and the y coordinate is the distance from the top wall. The $x1$ coordinate is the distance from the leading edge of the sidewall. The top wall was at y = 0 mm and the cowl surface was at y = 250 mm.

Fuel Supply Conditions

Nine tests from no. 12 to no. 20 were conducted in the present series. The timing for opening of each fuel supply valve was different, and so there were several kinds of fuel supply conditions in every test. The differences of combination of fuel flow rates in each test are represented by letters and each test condition is expressed by the test number and a letter, e.g., nos. 16d, 19e, 18d, etc. The operating condition with airflow only, i.e., with no fuel injection, is termed the reference condition. When there was fuel injection, the plasma ignitors were usually turned on.

One-Dimensional Calculation

Neither the pitot pressure measurement nor the gas sampling could be carried out in the engine or downstream of the engine in the present testing. Therefore, a one-dimensional flow calculation model was constructed to investigate the test results and estimate the model engine performances, for example, the Mach numbers in the engine model, the kinetic energy efficiency of the inlet, and the combustion efficiency. The assumptions and calculation conditions were as follows.

1) In the engine model of the one-dimensional calculation the effect of the swept angle was ignored and the distance from the leading edge $x1$ was used when the calculated results were compared with the experimental data.

2) In the calculation model a mass capture ratio of the inlet of 0.86 was chosen based on the spillage calculated by the two-dimensional shock-wave relation and the measured boundary-layer displacement thickness.[3] The definition of the mass capture ratio is as follows: (mass capture ratio) = (air mass flow rate at exit of the inlet)/(air mass flow rate with primary flow mass flux to the projected area at entrance of the engine).

3) The stream thrust function of the spilled air was set equal to that of the incoming airflow.[6]

4) The air and the combustion gas were equilibrium flows through the engine.

5) Modeling of mixing of fuel with the air was not done.

6) The hydrogen burned all at once in a stoichiometric condition with the specified combustion efficiency at the specified location. The location of heat release was estimated by the measured heat flux and wall pressure. The residual hydrogen mixed with the residual air.

7) The kinetic energy efficiency of the inlet and the combustion efficiency in the one-dimensional model were decided to show the similar distribution of the calculated wall pressure to that of the measured one.

8) The impulse function per unit cross section was conserved across the combustion.

9) The boundary layer was assumed to be turbulent throughout the engine and the friction coefficient was calculated with the formula of van Driest.[7]

10) The heat flux was calculated with the Reynolds analogy.

Results

The operating condition with airflow only is termed the reference condition. The reference condition was expressed as air in the figures.

Effect of Strut

Figures 2a–2d show wall pressure distributions with/without the short strut in the reference condition. In the figures, those of test no. 11 are also shown.[1,2] The fuel flow rate of test no. 11 is listed in Table 1. In Fig. 2d the scale of the wall pressure is different.

The pressure level with the strut was 1.5 times as high as that without the strut around the backward-facing step. On the top wall the level became higher than that without the strut. It can thus be seen that an increase in pressure was attained by attachment of the strut.

There was a pressure drop just downstream of the backward-facing step. The pressure behind the step seemed to be too high compared with other results.[8] This was a result of the difficulty in measuring very low pressure in the present testing, and also to the effect of the boundary layer. A thick boundary layer suppresses the decrease of pressure behind the step.[9] At y = 240 mm the pressure ratio increased downstream of the step. This was caused by shock-wave impingement.

The pressure level near the cowl was very high with or without the strut. The pressure first dropped at the entrance of the isolator and then increased downstream. The decrease was because of the expansion at the inlet–isolator corner on the sidewall, and the increase of the pressure was because of the shock wave from the leading edge of the cowl. The swept angle induces the downward flow toward the cowl and the open-bottom structure sustains the downward flow. According to the calculated results by the shock-wave relation, the airflow turns toward the cowl at 5 deg at the exit of the inlet. When

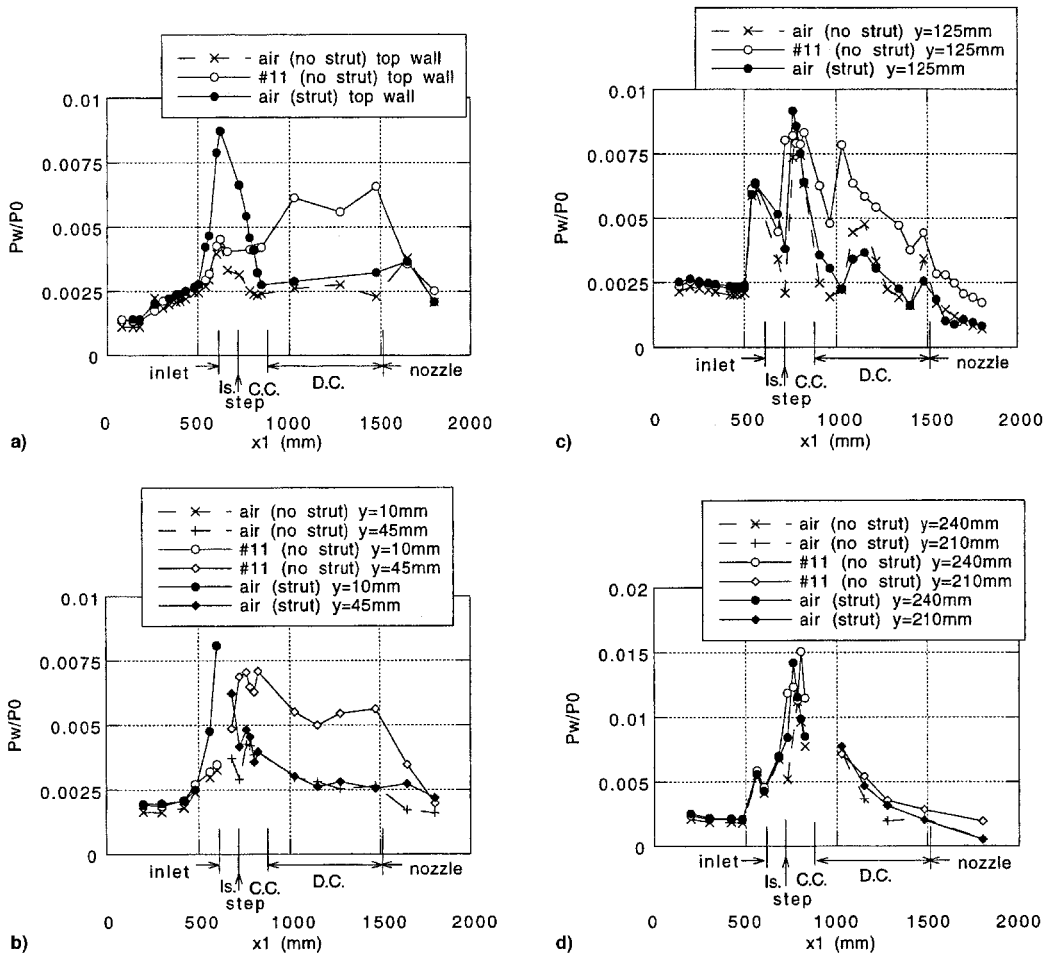

Fig. 2 Wall pressure with/without strut in airflow: a) on top wall, b) at y = 10 mm/45 mm, c) at y = 125 mm, and d) at y = 240 mm/210 mm.

the air recovers parallel to the cowl surface the pressure becomes 1.5 times as high as that upstream of the shock wave. In the experiment, around the step, the wall pressure at y = 240 mm/210 mm was about 1.5 times as high as that at y = 125 mm and agreed with the previous estimation.

According to the one-dimensional calculation, the kinetic energy efficiency of the inlet was estimated to be 0.992, which corresponded to a total pressure efficiency of 0.88. The kinetic energy efficiency of the present inlet was similar to the empirically estimated value of 0.997 by Waltrup et al.[10]

Engine Operating Mode

Wall Pressure

Figures 3a–3d show typical wall pressure distributions. In Fig. 3d the scale of the wall pressure is different. The fuel flow rates are listed in Table 1. In nos. 16d and 19e the wall pressure distributions in the inlet were the same as those of the reference condition; therefore, the model was in the start condition.

In no. 19e, the level of the wall pressure downstream of the step was much higher than that of the reference condition. The engine was in the intensive-combustion mode. At y = 240 mm/210 mm and at y = 125 mm, i.e., far from the top wall, the wall pressure was higher than that of the reference condition, even in the isolator. Though there was a pressure drop downstream of the backward-facing step at y = 240 mm, the pressure ratio was 1.3–1.6, meaning that there was a large, low-velocity region caused by combustion behind the step. Although there was a pressure drop at the step at y = 240 mm, the level of the wall pressure was much higher around the step than that of the reference condition. The large deflection angle on the cowl, which was caused by combustion, was estimated to be 22 deg from the wall pressure distribution at y = 240 mm.

The shock wave at the step at y = 240 mm passed $x1$ = 1100 mm/y = 125 mm and seemed to impinge at $x1$ = 1500 mm on the top wall. The second pressure peak around $x1$ = 1100 mm at y = 125 mm seemed to be caused by the shock wave, but the second peak around $x1$ = 1100 mm at y = 45 mm did not correspond to the location of the shock wave exactly. The second peak pressure around $x1$ = 1100 mm at y = 45 mm seemed to be caused by combustion.

In no. 16d the level of the wall pressure was slightly higher than that of the reference condition in the downstream part of the combustor and in the nozzle, especially around the top wall. The engine was in the weak-combustion mode. Although there was a pressure increase behind the step at y = 240 mm, the high-pressure region behind the step was short, and the pressure level was more similar to that of the reference condition than to that of no. 19e. There was no intensive heat release behind the step. According to the one-dimensional calculation, the combustion efficiency of no. 19e was 95%, whereas the efficiency of no. 16d was only 2%.

In no. 18d the mean pressure distribution in the inlet was different from that of the reference condition and the engine model was in the unstart condition. The pressure distribution on the top wall was similar to that on the sidewall, except at y = 240 mm. The deflection angle on the cowl becomes large because of the large flow-deflection toward the cowl in the inlet caused by the separation on the top wall, and there is a strong shock wave from the leading edge of the cowl. According to the pressure distribution in the inlet, the pressure ratio across the separation shock wave was 5, and the Mach

Table 1 Fuel flow rate and thrust by FMS

Test no.	Fuel flow rate, $g \cdot s^{-1}$ Normal	Top wall pilot	Sidewall pilot	Total	Equivalence ratio, total	Thrust (N), net
11 (no strut)	88	2.3	50	140.3	0.94	−900
16d	26	2.2	8.3	36.5	0.24	−980
19e	40	2.6	0	42.6	0.28	−250
18d (unstart)	67	2.9	8.9	78.8	0.53	−1150

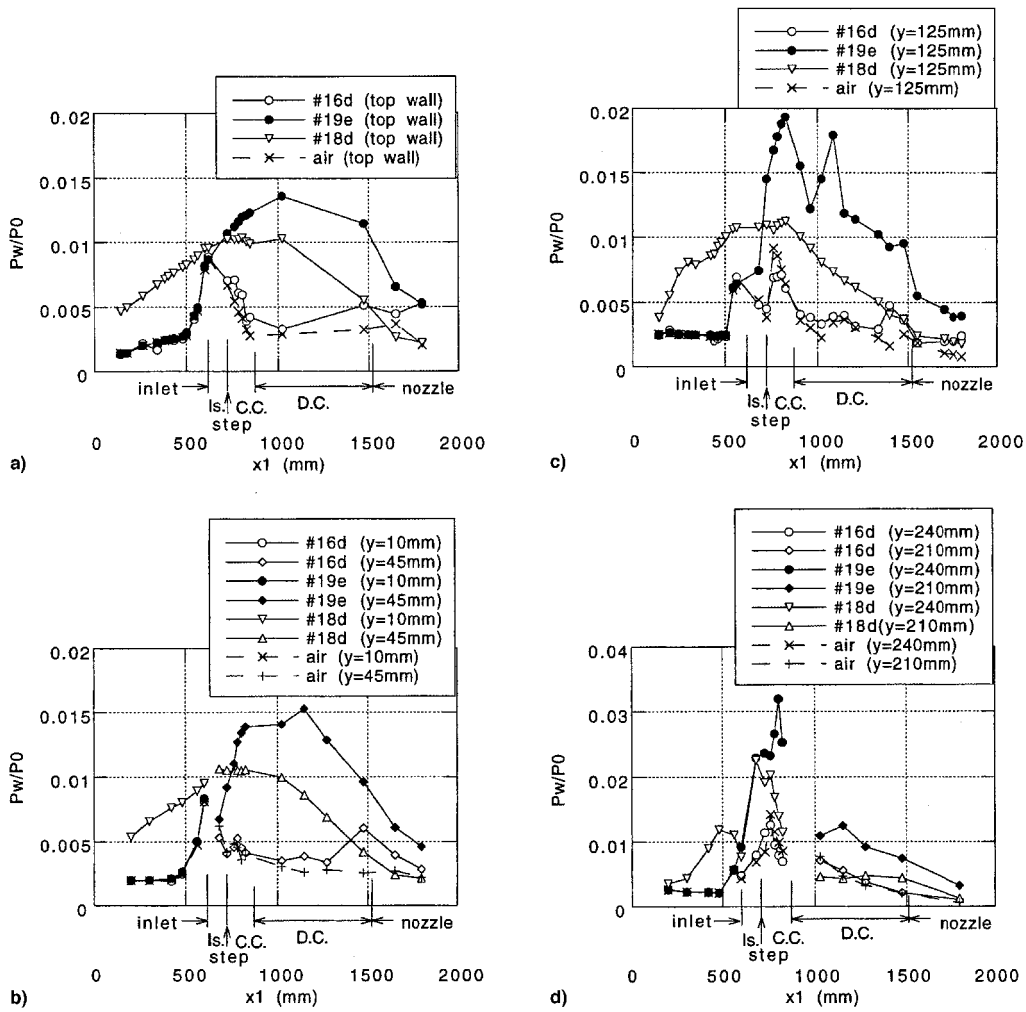

Fig. 3 Typical wall pressure distributions: a) on top wall, b) at y = 10 mm/45 mm, c) at y = 125 mm, and d) at y = 240 mm/210 mm.

number behind the shock wave was 3.6, respectively. The effect of the separation shock wave encompassed most of the inlet. Although the pressure was high in the inlet, it was much lower than the pressure after the normal shock wave. It would have been nondimensionalized pressure of 0.04, if the normal shock had existed at the entrance of the inlet.

Heat Flux

Figures 4a and 4b show the heat flux distributions. The heat flux can also increase upstream of combustion because of the increase of the heat transfer coefficient, but the effect of adiabatic wall temperature on heat flux is much greater than that of the heat transfer coefficient. The large heat flux indicates the location of combustion gas.

When the engine was in the intensive-combustion mode, as in no. 19e, the level of the heat flux was high in the combustor and in the nozzle. On the top wall the location of the first peak heat flux agreed with the step position. The wall pressure gradually increased, but the heat flux first decreased downstream of the first peak, then increased. The location of the second peak agreed with that of the second peak of the wall pressure. Because there was no impingement of a strong shock wave there, the large heat flux was caused by heat release, and the primary heat release occurred in the divergent part of the combustor on the top wall. On the top wall there were no primary fuel injection ports, and so fuel had to travel some distance from the sidewall to the top wall.

On the sidewall there was a shoulder point at the step and there was a peak point in the divergent part of the combustor. At y = 125 mm the second peak pressure at $x1$ = 1100 mm was similar to the first one at $x1$ = 800 mm; whereas the peak heat flux at $x1$ = 1000 mm was higher than the flux at $x1$ = 800 mm. On the other hand, according to the one-dimensional calculation of the intensive-combustion mode, the heat flux from the combustion gas was 2.2 $MW \cdot m^{-2}$, and that from the residual air was 0.7 $MW \cdot m^{-2}$ on the sidewall of the constant duct part of the combustor. The level of the measured heat flux on the sidewall was similar to that caused by the combustion

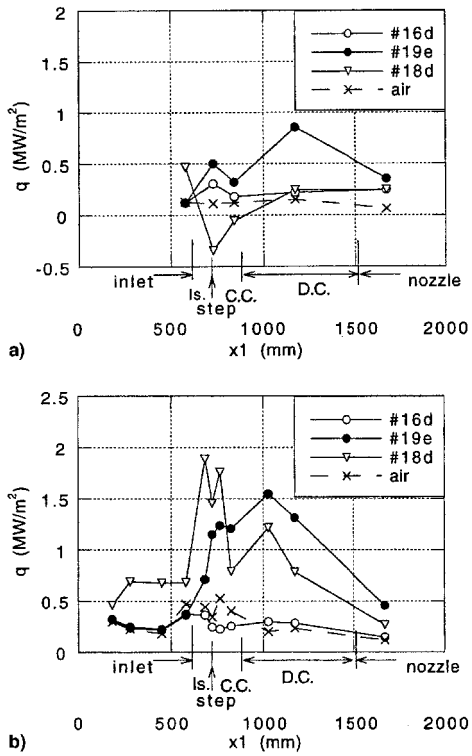

Fig. 4 Typical heat flux distributions: a) on top wall and b) at y = 125 mm.

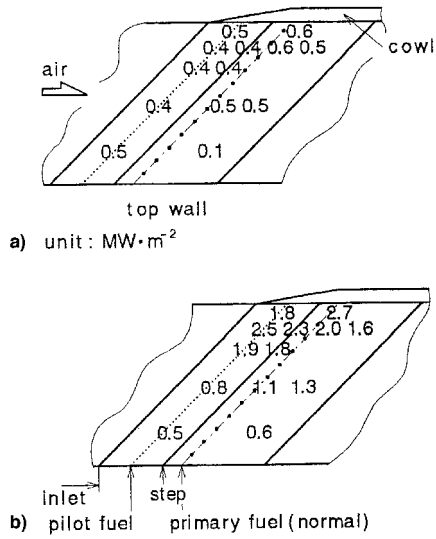

Fig. 5 Heat flux distributions: a) airflow (reference condition) and b) no. 19e (intensive combustion).

gas in the one-dimensional calculation. So there was primary heat release in the divergent part of the combustor.

Figures 5a and 5b show the heat flux distribution on the sidewall around the step. In the reference condition the heat fluxes were roughly uniform. In the intensive combustion of no. 19e, the heat fluxes were very high near the cowl, even upstream of the step. The heat flux increased downstream of the step near the top wall. The distribution agreed with the wall pressure distributions in Fig. 3.

After the plasma ignitors were turned off, the heat fluxes on the sidewall near the top wall were slightly smaller than those with operation of the plasma ignitors, while there was no change near the cowl. Once intensive combustion was attained, the effect of the plasma ignitors was limited in their vicinity and the flame was held, irrespective of the plasma ignitors.

As shown in Fig. 4, in no. 16d, the heat flux distribution on the top wall was slightly larger than that of the reference condition in the nozzle. It agreed with the wall pressure distribution of Fig. 3a. There was a small peak of heat flux around the step on the top wall, and such a peak was also observed in no. 19e. It seemed to be caused by the pilot fuel combustion by the plasma ignitors. On the sidewall, the heat flux level was lower around the step than that of the reference condition. The flame did not propagate from the top wall to the sidewall behind the step, and the sidewall was cooled by the unburned fuel.

In the unstart condition of no. 18d, the top wall was cooled around the step and the heat flux distribution resembled that of the reference condition downstream of the combustor on the top wall; whereas the heat fluxes were high around the step on the sidewall. In the inlet, the level of the heat flux was about four times as high as that of the reference condition. The wall pressure in Fig. 3c was also about four times as high as that of the reference condition. The increase of heat flux in the inlet in the unstart condition was a result of the increase of the pressure level, i.e., an increase of the heat transfer coefficient.

Force and Moment

Figure 6 shows the net engine thrust. The designations FMS and W.P. in Fig. 6 indicate the value measured by FMS and the value caused by the integration of the wall pressure, respectively. The integration of the wall pressure did not include the pressure on the strut. N+T and T represent a combination of normal injection and tangential injection of fuel, and tangential injection, respectively. The results for tangential injection are mentioned later. Table 2 lists the thrust, lift, and pitching moment of typical operating conditions.

Discrete changes in thrust level can be seen in Fig. 6. The thrust was large in the intensive-combustion mode in the narrow range of the fuel flow rate of about 50 $g \cdot s^{-1}$. There were two thrust levels for a fuel flow rate of 40 $g \cdot s^{-1}$, mentioned later in this paper. When the fuel flow rate was greater than 60 $g \cdot s^{-1}$, the engine was in the unstart condition. The unstart condition induced more drag than the reference condition. As shown in Fig. 3, this was because of the high-pressure level in the inlet and the moderate pressure level downstream of the combustor. According to the wall-pressure integration, the drag in the inlet was 1140 N in the unstart condition of no. 18d, while it was 490 N in the start condition of no. 19e. According to the one-dimensional calculation results the friction drag and pressure drag acting outside of the sidewall were estimated to be 260 N. The net, positive engine thrust was estimated by compensating the drag acting outside of the sidewall for the measured thrust by FMS in the intensive-combustion mode.

In the intensive-combustion mode the lift was negative. The pressure around the cowl was very high in the vicinity of the step, indicating that the large force on the cowl canceled the lifting force in the inlet. In the weak-combustion mode there was weak combustion around the top wall in the divergent part of the combustor, so that the lift was slightly larger than that

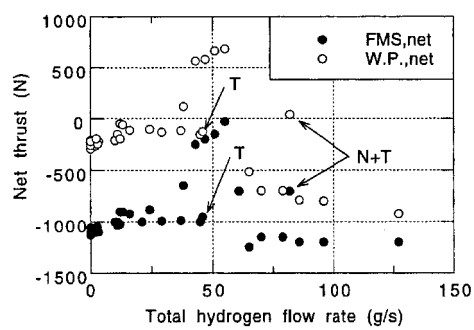

Fig. 6 Net thrust.

Table 2 Net thrust, lift, and pitching moment by FMS

Test no.	Fuel flow rate, $g \cdot s^{-1}$, total	Net thrust, N	Lift, N	Pitching moment, N-m
Air only	——	−1100	300	750
16d (weak combustion)	36.5	−980	600	500
19e (intensive combustion)	42.6	−250	−200	1700
18d (unstart)	78.8	−1150	1500	1450

Table 3 Fuel flow rate and thrust by FMS in the intensive-combustion mode

	Fuel flow rate, $g \cdot s^{-1}$					
Test no.	Normal	Top wall pilot	Sidewall pilot	Total	Equivalence ratio, total	Thrust (N), net
19e	40	2.6	0	42.6	0.28	−250
20d	36	2.3	8.4	46.7	0.31	−200
19d	40	2.6	8.8	51.4	0.34	−150
14e	53	2.3	0	55.3	0.37	−30

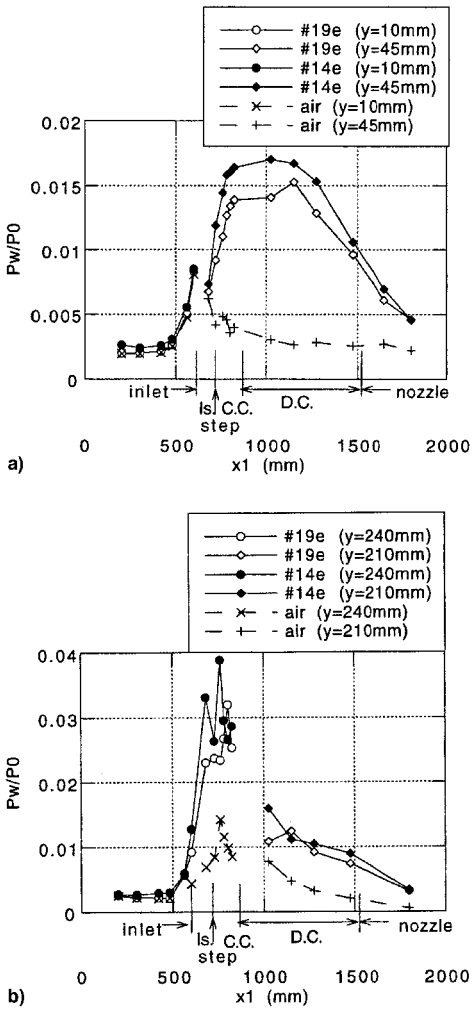

Fig. 7 Wall pressure distribution in intensive-combustion mode: a) at y = 10 mm/45 mm and b) at y = 240 mm/210 mm.

of the reference condition. In the unstart condition the lift became very large because of the high pressure in the inlet.

The pitching moment was positive in every test, even in the reference condition. This was because of the high pressure at the step near the cowl and the bottomless shape of the inlet. In the intensive-combustion mode the large force acted on the cowl in the y direction, and thus the pitching moment became large. In the unstart condition the pitching moment was also large because of the high-pressure level in the inlet. In the weak-combustion mode the pressure on the top wall was slightly larger than that of the reference condition in the divergent part of the combustor and in the nozzle, and so the pitching moment was slightly smaller than that seen in the reference condition.

Intensive Combustion

Effect of Fuel Flow Rate

There were four operations of the intensive-combustion mode in the present testing. The fuel flow rates and the thrust are listed in Table 3. Figures 7a and 7b show wall pressure distributions of nos. 19e and 14e. Within the intensive-combustion mode the fuel flow rate was smallest in no. 19e and largest in no. 14e.

The level of the wall pressure in the combustor increased with the fuel flow rate. The heat release seemed to increase with the fuel flow rate. The pressure distribution in the isolator at y = 10 mm/45 mm was similar to that of the reference condition. The level of the sidewall pressure at y = 240 mm/210 mm was very high around the step and was already higher than that of the reference condition in the isolator.

Effects of Fuel Injection Method

In test no. 20, as shown in Table 4, the usage of only the normal injection of the primary fuel was not able to attain intensive combustion in no. 20c. The addition of the sidewall pilot fuel resulted in the intensive combustion in no. 20d. The concentration of the fuel or the total fuel flow rate also seemed to be important in the vicinity of the step.

On the other hand, in the present testing, the intensive combustion in nos. 19e and 20d and the weak combustion in no. 12c were observed at the same total fuel flow rate of around 45 $g \cdot s^{-1}$ as shown in Table 4 and Fig. 6. Almost all of the fuel was injected downstream of the step in nos. 19e and 20d, while it was injected upstream of the step in no. 12c. Although the concentration of the fuel around the step was important the normal fuel injection downstream of the step was indispensable for attaining intensive combustion.

In the present testing, tangential fuel injection was investigated in only one test, i.e., no. 20. The fuel flow rate rates are shown in Table 5. The net thrust decreased with the tangential injection of fuel as shown in Fig. 6 and Table 5. The thrust produced by the tangential, unburned gas injection was about 100 N in nos. 20e and 20f. The decrease of drag in no. 20f was mainly caused by the gas injection. Figure 8 shows the wall pressure distributions. The wall pressure distributions with the tangential injection were almost the same as those of no. 16d. When the normal fuel injection was also used with

Table 4 Fuel flow rate and thrust by FMS

Test no.	Fuel flow rate, g·s^{-1} Normal	Top wall pilot	Sidewall pilot	Total	Equivalence ratio, total	Thrust (N), net
20c	36	2.3	0	38.3	0.26	−650
20d	36	2.3	8.4	46.7	0.31	−200
19e	40	2.6	0	42.6	0.28	−250
12c	0	3.1	42	45.1	0.30	−1000

Table 5 Fuel flow rate and thrust by FMS

Test no.	Fuel flow rate, g·s^{-1} Normal	Tangential	Top wall pilot	Sidewall pilot	Total	Equivalence ratio, total	Thrust (N), net
20d	36	0	2.3	8.4	46.7	0.31	−200
20e	36	35	2.3	8.4	81.7	0.54	−700
20f	0	35	2.3	8.4	45.7	0.30	−950

Table 6 Fuel flow rate and thrust by EMS

Test no.	Fuel flow rate, g·s^{-1} Normal	Top wall pilot	Sidewall pilot	Total	Equivalence ratio, total	Thrust (N), net
14d	53	2.3	9.7	65.0	0.43	−1250
14e	53	2.3	0	55.3	0.37	−30

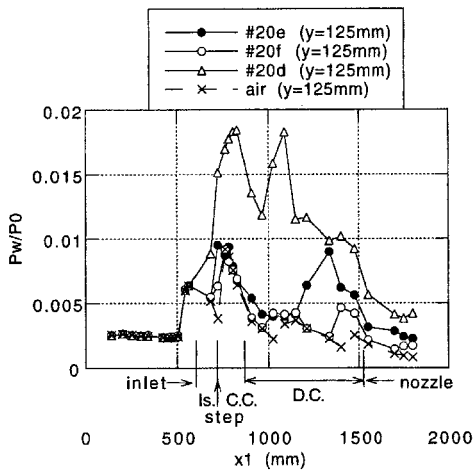

Fig. 8 Wall pressure at y = 125 mm in tangential fuel injection.

the tangential injection in no. 20e, the level of the pressure was higher in the combustor than when only the tangential fuel injection was used in no. 20f.

Restart

In test no. 14 the engine moved from the unstart condition of no. 14d to the start condition of no. 14e when injection of the sidewall pilot fuel of 9.7 g·s^{-1} was stopped (Table 6). There was no difficulty in changing from the unstart to the start condition.

Discussion

Intensive Combustion

The mechanism of the intensive combustion, which produced thrust, is discussed first. Intensive combustion was attained with the following conditions: 1) usage of a short strut, 2) normal fuel injection downstream of the step, and 3) a suitable fuel flow rate.

Role of Strut

As shown in Figs. 2a–2d, when a large amount of fuel was injected normally in the model with no strut as in no. 11, there was no pressure drop at the step, and the pressure level was similar to or higher than that of the reference condition with the strut on the sidewall. However, the pressure level on the top wall around the step was low even with such a high fuel flow rate in the model with no strut, and the level was 0.5 times as low as that of the reference condition with the strut. A pressure increase around the step was attained by the usage of a strut around the fuel injector. According to results of the inlet testing with the strut, there was a large, disturbed, low-velocity region around the foot of the strut.[11] Such a region with high pressure was necessary for the initiation of intensive combustion. However, the conditions were not sufficient to attain intensive combustion because there was a weak-combustion mode even with the strut.

Flame Propagation in Low-Velocity Region

In the design procedure of the original engine model that had a strut,[2] the length from the step to the fuel injector of 20 mm, which was five times as large as the height of the step, was determined to avoid interaction between the separated boundary layer and the fuel injected behind the reattachment of the boundary layer.[12,13] The recirculation region behind the step was designed to be used for flame holding of the pilot fuel. The avoidance of the interaction seemed to be necessary for preventing the gas behind the step from reaching an overly dense fuel condition and becoming too cool.

Conditions 2 and 3 created a high-pressure, low-velocity region between the backward-facing step and the normal fuel injection holes on the sidewall by the interaction between the boundary layer and the injected fuel.[14] The designed configuration of the step-injector location was not suitable for the Mach 6 operation. In the present testing the interaction was necessary for the intensive combustion. Creation of the interaction was insufficient, however, because there was a low-velocity region even in the weak-combustion mode and in the engine with no strut, as shown in Fig. 2d. The location and the size of the low-velocity region are important.

Table 7 Normally injected fuel jet geometry without chemical reaction[a]

Fuel flow rate per injection port, $g \cdot s^{-1}$	Mach number	Mach disk location (distance, height)	Fuel jet diameter at Mach disk	Detachment length
2.8 (no strut)	4.0	(2.8, 2.3)	2.2	0.6
2.1 (strut, intensive-combustion mode)	3.6	(2.3, 1.9)	1.9	0.5
1.3 (strut, weak-combustion mode)	3.6	(1.8, 1.5)	1.5	0.4

[a]Unit = millimeters.

The flame probably propagated in the low-velocity region from the top wall to the cowl in the intensive-combustion mode. In the weak-combustion mode, there was a pressure drop at the step on the sidewall at y = 10 mm/45 mm; this means that there was no large, low-velocity region behind the step there. Thus, the flame did not propagate to the cowl. Once the flame was propagated near the cowl, a large, low-velocity region was created there by combustion and the flame was sustained, even after the plasma ignitors were turned off.

Possibility of a Large, Low-Velocity Region

To examine the possibility of the existence of a large, low-velocity region at the step, the locations of the center of the Mach disk in the normally injected fuel jet and the diameters of the fuel jet at the Mach disk position without chemical reaction were calculated with the model by Billig et al.,[15] the results are shown in Table 7. The coordinates of the Mach disk location were the distance from the injection hole and the height from the wall surface. To estimate the upstream or y-direction propagation of the downstream flow structure change, the detachment length of the shock wave caused by the injected fuel was also calculated with the Billig's model.[16] The fuel jet was assumed to be a cylinder with the diameter of the fuel jet at the Mach disk position. The calculated diameter is also shown in Table 7. In the calculation the Mach number and other properties of the primary flow were those of the one-dimensional calculation.

According to the calculated results, the penetration lengths, the detachment lengths, and the fuel jet diameters were very small. There must be no interaction between the boundary layer and the injected fuel on the sidewall in such flow conditions as those listed in Table 7.

The boundary-layer thickness of 99% velocity was 58 mm at the entrance of the engine model,[3] and the fuel injection port nearest the top wall, located at y = 10 mm, seemed to be in the boundary layer. Moreover, when there was a strut, a low-velocity region was created around its foot.[11] Therefore, the injection port was in the low-velocity region. When the fuel is injected into a low Mach number flow, the detachment length, the diameter of the fuel jet, and the difference of the detachment length because of the fuel flow rate all increase. For example, when the Mach number at the injection port is 1.4, the detachment lengths of the intensive-combustion mode and the weak-combustion mode are 9 and 7 mm, respectively. The diameters of the fuel jet of the combustion modes are 4.5 and 3.5 mm, respectively, and the difference of the lengths and the diameters are enlarged. Meanwhile, the reattachment length of the boundary layer over the backward-facing step increases with the thickness of the incoming boundary layer,[9] i.e., with growth of the low-velocity region. The attachment of the strut caused the interaction between the fuel injection and the reattaching boundary layer, and the interaction created a large, low-velocity region between the step and the fuel injection port. The interaction also spread in the y direction on the sidewall near the top wall.

The tangential injection blew off the low-velocity region around the step and the flame was no longer anchored. The operating mode thus changed to the weak-combustion mode. Tangential injection with the present fuel flow rates was not suitable for the present engine configuration or for the present engine-operating conditions.

Combustion Efficiency

In the intensive-combustion mode, there was probably a wide, low-velocity region around the step, especially around the cowl. Mixing and combustion probably occurred around the low-velocity region and this resulted in an anchored flame and high combustion efficiency.

In the weak-combustion mode the pilot fuel flow rate from the top wall was about 6% of the total fuel flow rate and the value was similar to that of the estimated combustion efficiency of 2%. Therefore, most of the combusted fuel seemed to be the pilot fuel injected from the top wall. There was no large, low-velocity region on the sidewall in the weak-combustion mode, and there was no residence time for mixing and reaction around the step. Furthermore, there was no ignition source on the sidewall. The combustion observed in the nozzle in the weak-combustion mode was caused by self-ignition after supersonic mixing.

Unstart Condition

Initiation of Unstart

In Mach 4 testing of inlets[17] and in the Mach 4 testing in the RJTF,[1,2] gradual transition from the start condition to the unstart condition was observed; it clearly appeared in the top-wall pressure distribution. In the present Mach 6 testing, such gradual transition was not observed.

When the swept angle was small, the change from a start to an unstart condition abruptly occurred in the Mach 4 flow condition.[17] In the present testing, the inflow Mach number of 5.3 was higher than 4, and the effect of the swept angle became smaller than that in the Mach 4 flow condition. Therefore, there was a possibility of abrupt change of the inlet condition caused by the high Mach number.

The wall pressure in the isolator at y = 10 mm/45 mm did not change with the increase of the fuel flow rate in the intensive-combustion mode, while that at y = 240 mm/210 mm greatly increased with the fuel flow rate. In the region with increased pressure, there was a thick, low-velocity region on the wall. Therefore, the low-velocity region seemed to grow from the cowl with the increase of the fuel flow rate, and the low-velocity region seemed to reduce the substantial cross section, and/or to interact with the boundary layer on the sidewall to induce the large separation.

The length of the isolator was designed to avoid the inlet-combustor interaction in the lowest Mach number condition at the RJTF, i.e., the Mach 4 flight condition, in which the pressure increase was anticipated to reach the most upstream point in the isolator.[18,19] As planned in the design procedure, in the present Mach 6 testing, the large pressure increase in the isolator was not observed in the start condition, except around the cowl. In the designing procedure, the strong, inlet–isolator–cowl interaction enhanced by the combustion, which appeared in the present testing, was unforeseeable. One of the reasons for the narrow region of the start condition was the interaction around the cowl. To enlarge the start condition with greater fuel flow rates, several improvements are possible, e.g., elongation of the isolator, change of the combustor configuration, and suitable distribution of the injected fuel. Elongation of the isolator and change of the combustor are under investigation.[20,21]

Restart

In test no. 14 the engine condition suddenly changed from the unstart to the start condition because of the reduction of the fuel flow rate. Good restartability is apparently caused by the swept angle and the open-bottom structure of the inlet. When there is a swept angle the leading edge of the cowl is located far downstream of the exit of the inlet on the top wall. Therefore, the substantial open area of the inlet is wide with the swept angle and the excess fluid can spill out easily in the unstart condition. The adoption of the swept angle and the open-bottom structure will be necessary for design of scramjet engines. For a ramp-compression-type inlet, a substitute mechanism for the swept angle and the open-bottom structure is necessary for good startability.

High Pressure Around Cowl

The high pressure around the cowl in the reference condition was because of the swept angle and the open-bottom structure of the inlet, and there was probably a wide, low-velocity region there. Once the combustion was initiated there, the flame was probably easily held, and the pressure further increased. However, the swept angle and the open-bottom structure were necessary for good startability. Pressure distribution is inevitable for an engine with a swept angle. The flow distortion to the combustor is inevitable in all scramjet engines because of the restriction of the engine length, the transitions of the inflow Mach number and the shock-wave positions, and the existence of a boundary layer and an entropy layer.

Concluding Remarks

A subscale scramjet engine model with a short strut was tested under Mach 6 flight conditions in the RJTF. The following points were clarified:

1) Addition of a short strut was effective for intensive combustion.

2) There were three modes of engine operation with normal fuel injection: a) with a low level of fuel flow rate weak combustion mainly occurred in the divergent part of the combustor with very small production of thrust; b) with a high level of fuel flow rate within the start condition intensive combustion occurred in the combustor with high combustion efficiency; and c) when the normally injected fuel flow rate was excessive the engine was in the unstart condition, the drag was greater than that in the condition with airflow only.

3) The flame was held in the low-velocity region around the step in the intensive-combustion mode, especially near the cowl. The flame could be held without the plasma ignitors.

4) Tangential injection with the fuel flow rates employed here was not suitable for the present engine configuration or for the present engine operating conditions.

5) In the inlet gradual transition from the start to the unstart condition was not observed. Unstart seemed to begin with growth of the low-velocity region around the cowl. Restart from the unstart condition was observed when the fuel flow rate was reduced.

Acknowledgments

The authors thank the members of the scramjet research group of the National Aerospace Laboratory for cooperation in testing, data processing, and discussion. The present study was conducted as a part of the program of the National Aerospace Laboratory–Mitsubishi Heavy Industries, Ltd., cooperative research.

References

[1]Yatsuyanagi, N., Chinzei, N., and Miki, Y., "Initial Tests of a Subscale Scramjet Engine," *Proceedings of the 12th International Symposium on Air Breathing Engines* (Melbourne, Australia), AIAA, Washington, DC, 1995, pp. 1330–1337.

[2]Masuya, G., and Chinzei, N., "Scramjet Engine Tests at Mach 4 and 6," The International Union of Theoretical and Applied Mechanics Symposium on Combustion in Supersonic Flows 7, Poitiers, France, Oct. 1995.

[3]Hiraiwa, T., Mitani, T., Izumikawa, M., and Ono, F., "Calibration Studies of Nozzle Flow in Ramjet Engine Test Facility," The 20th International Symposium on Space Technology and Science, Committee of International Symposium on Space Technology and Science, Paper 96-d-14, Gifu, Japan, May 1996.

[4]Masuya, G., Kudo, K., Murakami, A., Komuro, T., Tani, K., Kanda, T., Wakamatsu, Y., Chinzei, N., Sayama, M., Ohwaki, K., and Kimura, I., "Some Governing Parameters of Plasma Torch/Flame-Holder in a Scramjet Combustor," *Journal of Propulsion and Power*, Vol. 9, No. 2, 1993, pp. 176–181.

[5]Carslaw, H. S., and Jaeger, J. C., *Conduction of Heat in Solids*, 2nd ed., Oxford Univ. Press, Oxford, England, UK, 1959, pp. 112, 113.

[6]Kanda, T., Tani, K., Komuro, T., Murakami, A., Kudo, K., and Chinzei, N., "Impulse Function and Drag in Scramjet Inlet Models," *Journal of Propulsion and Power*, Vol. 12, No. 6, 1996, pp. 1181–1183.

[7]White, F. M., *Viscous Fluid Flow*, McGraw–Hill, New York, 1974, pp. 632–640.

[8]Lamb, J. P., and Oberkampf, W. L., "Review and Development of Base Pressure and Base Heating Correlations in Supersonic Flow," *Journal of Spacecraft and Rockets*, Vol. 32, No. 1, 1995, pp. 8–23.

[9]Karashima, K., and Hasegawa, K., "An Approximate Approach to Base Flow Behind Two-Dimensional Rearward-Facing Steps Placed in a Uniform Supersonic Stream," Inst. of Space and Aeronautical Science, Rept. 501, Tokyo, Japan, Nov. 1973.

[10]Waltrup, P. J., Billig, F. S., and Stockbridge, R. D., "Engine Sizing and Integration Requirements for Hypersonic Airbreathing Missile Applications," CP-307, AGARD, 1982.

[11]Tani, K., Kanda, T., Kudo, K., Murakami, A., Komuro, T., and Itoh, K., "Aerodynamic Performance of Scramjet Inlet Models with a Single Strut," AIAA Paper 93-0741, Jan. 1993.

[12]Diskin, G. S., and Northam, G. B., "Effect of Scale on Supersonic Combustor Performance," AIAA Paper 87-2164, June 1987.

[13]Wagner, T. C., O'Brien, W. F., Northam, G. B., and Eggers, J. M., "Design and Evaluation of a New Injector Configuration for Supersonic Combustion," *Proceedings of the 8th International Symposium on Air Breathing Engines* (Cincinnati, OH), AIAA, New York, 1987, pp. 390–397.

[14]Huber, P. W., Schexnayder, C. J., Jr., and McClinton, C. R., "Criteria for Self-Ignition of Supersonic Hydrogen-Air Mixtures," NASA TP-1457, 1979.

[15]Billig, F. S., Orth, R. C., and Lasky, M., "A Unified Analysis of Gaseous Jet Penetration," *AIAA Journal*, Vol. 9, No. 6, 1971, pp. 1048–1057.

[16]Billig, F. S., "Shock-Wave Shapes Around Spherical- and Cylindrical-Nosed Bodies," *Journal of Spacecraft and Rockets*, Vol. 4, No. 6, 1967, pp. 822, 823.

[17]Tani, K., Kanda, T., and Tokunaga, T., "Starting Characteristics of Scramjet Inlets," *Proceedings of the 11th International Symposium on Air Breathing Engines* (Tokyo, Japan), AIAA, Washington, DC, 1993, pp. 1071–1080.

[18]Chinzei, N., Komuro, T., Kudou, K., Murakami, A., Tani, K., Masuya, G., and Wakamatsu, Y., "Effects of Injector Geometry on Scramjet Combustor Performance," *Journal of Propulsion and Power*, Vol. 9, No. 1, 1993, pp. 146–152.

[19]Waltrup, P. J., and Billig, F. S., "Prediction of Precombustion Shock Wall Pressure Distributions in Scramjet Engines," *Journal of Spacecraft and Rockets*, Vol. 10, No. 9, 1973, pp. 620–622.

[20]Sunami, T., Sakuranaka, N., Tani, K., Hiraiwa, T., and Shimura, T., "Mach 4 Tests of a Scramjet Engine—Effect of Isolator," The AIAA 13th International Symposium on Air Breathing Engines, Chattanooga, TN, Sept. 1997.

[21]Sato, S., Izumikawa, M., Tomioka, S., and Mitani, T., "Scramjet Engine Test at the Mach 6 Flight Condition," AIAA/ASME/SAE/ASEE 33rd Joint Propulsion Conf., Seattle, WA, July 1997.